Article ID：1007−7294(2026)06−0970−14

Experimental and Numerical Study on Mechanical Properties of Three-dimensional Plate-frame and Truss Honeycomb

LI Qian−ning[1,2,3], *XU Lin−zhi*[3], *ZHANG Yi−heng*[1,2,3], *HU Peng−cheng*[1,2,3], *WU Wen−hua*[4], *LI Chun−bao*[1,2,3], *CHEN Wei*[1,2,3], *LI Pu*[5,6], *LI Xiao−bin*[1,2,3]

(1. Ship Shock Damage and Safety Protection Key Discipline and Technology Research Center, Wuhan University of Technology, Wuhan 430063, China; 2. Ship Impact and Protection of Hubei Province Key Discipline Laboratory Wuhan University of Technology, Wuhan 430063, China; 3. School of Naval Architecture, Ocean and Energy Power Engineering, Wuhan University of Technology, Wuhan 430063, China; 4. State Key Laboratory of Structural Analysis, Optimization and CAE Software for Industrial Equipment, Dalian University of Technology, Dalian 116024, China; 5. China Ship Development and Design Center, Wuhan 430064, China; 6. National Key Laboratory on Ship Vibration and Noise, Wuhan 430033, China)

Abstract: With in-depth research on honeycomb structures for ship protection, diverse 3D honeycomb configurations have emerged. This paper aims to explore the traits of different 3D honeycomb designs and offer ideas for the future structural layouts. Both experimental tests and numerical analysis on the mechanical properties of 3D plate-frame and truss honeycombs were carried out. The test samples, made of nylon via laser sintering in an additive manufacturing process, underwent quasi-static compression tests to uncover the disparities in deformation patterns between the two honeycombs. By closely examining typical cell deformations during compression, the differences in failure modes were revealed. Because the load-bearing capacity of a structure and its density, the authors while studying these two types of honeycombs, also explored the relationship between the specific stiffness and nominal density of various typical 2D and 3D structures. Finally, a parametric analysis was performed to assess the impact of internal concavity angles, cell thicknesses, and materials on mechanical properties.

Key words: cellular solids; compression testing; additive manufacturing; negative Poisson's ratio; plate-frame and truss honeycomb

CLC number: U663.7 **Document code:** A **doi:** 10.3969/j.issn.1007−7294.2026.06.009

0 Introduction

With the rapid growth in shipping, aerospace, and automotive sectors, traditional materials and structures struggle to meet the increasingly intricate requirements. Metamaterials, boasting outstanding properties, hold extensive application prospects. As a crucial structure for fastening marine equipment, the marine pedestal plays a key role in preventing the direct transmission of the loads from the ship hull to the equipment. With the traditional pedestal design, it is difficult to achieve a balance between the load-bearing capacity and the anti-

Received date：2025−09−18

Foundation items：State Key Laboratory of Structural Analysis, Optimization and CAE Software for Industrial Equipment (GZ25121); National Key Laboratory on Ship Vibration and Noise (6142204220301)

Biography：LI Qian-ning (2001−), male, master, E-mail: whut_lqn@163.com;
LI Chun-bao (1988−), male, assistant professor, corresponding author, E-mail: leecubao@whut.edu.cn.

impact performance. Moreover, the protective performance is usually in a positive correlation with the self-weight of the structure, which runs counter to the design concept of lightweight protection pursued for modern equipment. In view of this, the research and development of more lightweight and efficient protective structures have already become a high-profile research focus in the field of ship protection, and it is of vital significance for promoting the innovation and development of ship protection technologies.

Metamaterials are man-made, achieving outstanding properties not found in natural materials through structural design rather than chemical composition. Many of these structures, like honeycomb materials with internal voids, possess remarkable protective capabilities. When subjected to pressure and entering the plastic stage, the stable stress endows them with excellent impact resistance. Previous research indicates that modifying honeycomb cell structures can induce a negative Poisson's ratio effect, enhancing mechanical properties such as compressive capacity[1], shear modulus[2−3], fracture toughness[4−5], impact resistance[6−7], and specific energy absorption[8−9]. In 1982, Gibson et al[10] first proposed a 2D re-entrant hexagonal honeycomb with a negative Poisson's ratio. Since then, scholars have explored diverse negative Poisson's ratio structures[11], with the re-entrant structure standing out due to its excellent performance. Theocaris et al[12] introduced a star-shaped variant, Grima et al[13] proposed different symmetric star-shaped structures, Wang et al[14−15] combined shapes to create re-entrant star-shaped honeycombs with better impact resistance and designed star-arrow honeycombs, Qiao et al[16−17] investigated crushing of tensile expansion structures and formulated theoretical equations, Wei et al[18−20] devised a star-triangle honeycomb and probed collapse mechanisms, and Wang et al[21] incorporated the gradient concept, confirming its potential to enhance honeycomb mechanical performance.

Previously, experimental research was mostly confined to two-dimensional honeycombs due to processing constraints. However, with the advancement of 3D printing, complex 3D models can now be fabricated via laser sintering and electron beam melting. Yang et al[22] used electron-beam melting to produce 3D re-entrant titanium alloy structures, and analyzed the damage. Beharic et al[23] made three types of 3D honeycomb sandwich structures from nylon 12 by laser sintering, and studied geometric impacts on energy absorption via drop hammer tests. Guo et al[24] fabricated four kinds of honeycomb tubes from nylon using laser sintering, and studied geometry effects on Young's modulus, peak force, energy absorption, and damage modes. Gao et al[25] analyzed how parameters affect the impact resistance of 3D double-arrow honeycombs for crash box design guidance. Guo and Yang et al[26−28] proposed a new 3D double U-shaped negative Poisson's ratio structure, which has a higher mechanical property-to-weight ratio. Wang et al[29] designed a 3D re-entrant lattice structure, demonstrating significant negative Poisson's ratio characteristic. Wang et al[30] developed a theoretical model of a 3D re-entrant honeycomb using the energy method to deduce its Poisson's ratio and Young's modulus. Compared to 2D honeycombs, 3D ones are lighter and more impact-resistant, drawing more attention on their mechanical properties.

Although previous scholars have proposed numerous three-dimensional configurations, the impact of configuration characteristics on structural performance remains underexplored. Unlike two-dimensional honeycomb, which is simply stretched out-of-plane from a planar graph, three-dimensional honeycomb can be constructed in two main ways: stretching the planar model into plate members for orthogonal splicing, or directly splicing thin rods in 3D space. Herein, the honeycombs made by these methods are termed panel-frame and truss honeycombs, respectively. Different configurations typically lead to varying deformation patterns and mechanical properties. In this study, two negative Poisson's ratio honeycomb structures, plate-frame and truss, were designed. These models were 3D-printed to explore performance differences due to configuration. This study can provide reference for the selection of protective structures in different circumstances. Based on experimental and numerical results, the compression performance and failure mechanisms of both honeycombs were comparatively analyzed.

1 Model fabrication and testing

1.1 Model design and fabrication

The design parameters of two 3D negative Poisson's ratio honeycomb structures are shown in Tab.1 and Fig.1. These two structural forms are typical three-dimensional configurations of re-entrant hexagons. The difference is that plate-frame honeycomb cells must extend outward and then be orthogonally joined. Due to the concave angle, the structure contracts under compression, generating a negative Poisson's ratio effect in both types. Given the 3D honeycomb's complexity, advanced manufacturing like Selective Laser Sintering (SLS) is needed. The model is fabricated with Nylon 12 using an HP Jet Fusion 5200 3D Printer. During the manufacturing process, a high-power laser is used to completely melt the surface layer of the nylon powder, on top of which layer-by-layer processing is carried out until the sample is complete. This operation can avoid defects in the material structure and maximize the performance potential of the material.

Tab.1 Design parameters of the honeycomb structures

Structure	l_1/mm	l_2/mm	θ/°	t/mm	b/mm
Plate-frame honeycomb	25	10	70	1.5	5
Truss honeycomb	25	10	70	2.5	—

1.2 Test platform

In order to explore the deformation patterns and mechanical properties of the two honeycombs, quasi-static compression tests (Fig.2) were carried out on the two honeycomb specimens by utilizing an electronic universal testing machine in this study. The machine consists of two parts: the operating system and the test machine. The operating system controls the compression speed and stores the relevant data during the test, and the test machine is responsible for the compression of the test specimen. The type of electronic universal testing machine used for testing was WDW-300, with a maximum compressive force of up to 300 kN and a test speed of 1 mm/min.

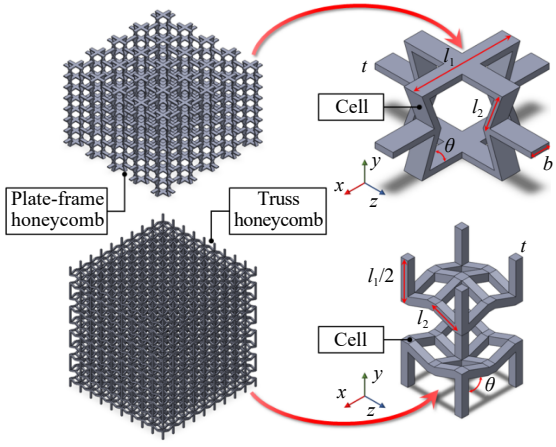


Fig.1 Design models of plate-frame and truss honeycomb

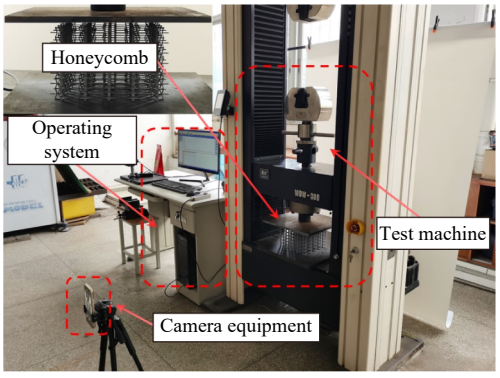


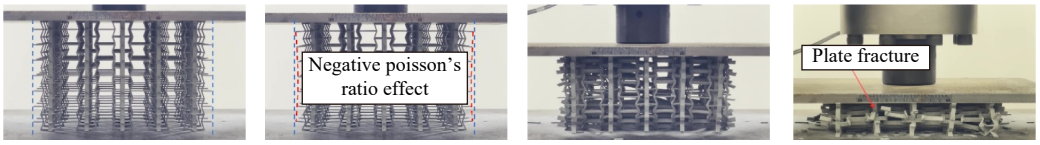
Fig.2 Quasi-static compression test equipment

1.3 Analysis of test results

1.3.1 Plate-frame honeycomb

The deformation process of the plate-frame honeycomb is shown in Fig.3. At the initial phase of pressurization, the whole structure is in the elastic stage. Because of the internal concave angle, the inclined walls rotate around the nodes, causing overall contraction and a negative Poisson's ratio effect. Due to the friction factor between the honeycomb and the panels, the contraction mainly concentrates in the middle. As stress increases, the inclined walls start to yield, and some plates fracture. The plate-frame honeycomb's

compression process is stable, with moderate plate damage and failure. With further compression, the plates overlap and the honeycomb gets crushed.



（a）Initial stage　（b）Elastic stage　（c）Plateau stage　（d）Densification stage

Fig.3 Deformation process of plate-frame honeycomb

The stress-strain curve of the plate-frame honeycomb's quasi-static compression process is shown in Fig.4. The curve can be mainly divided into three stages: linear elastic, plateau, and densification. In the initial compression stage, the honeycomb mostly undergoes elastic deformation, with the stress increasing linearly. Then, it enters the plastic deformation stage where inclined cell walls yield. Due to nylon's brittleness, many cell walls crack, and the stress drops rapidly. As the fracture behavior stabilizes, the stress levels off, forming a relatively flat plateau stage, where stress values slightly fluctuate due to cell wall fracture damage. As the strain increases, the honeycomb reaches the densification stage, and the stress rises rapidly.

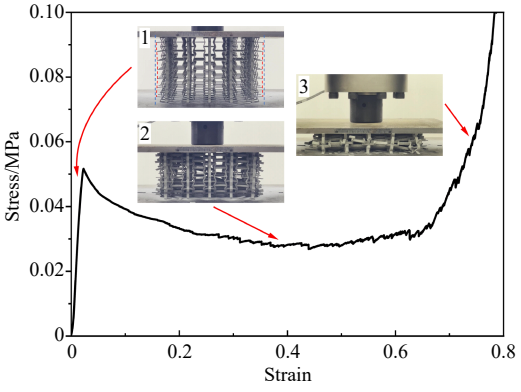
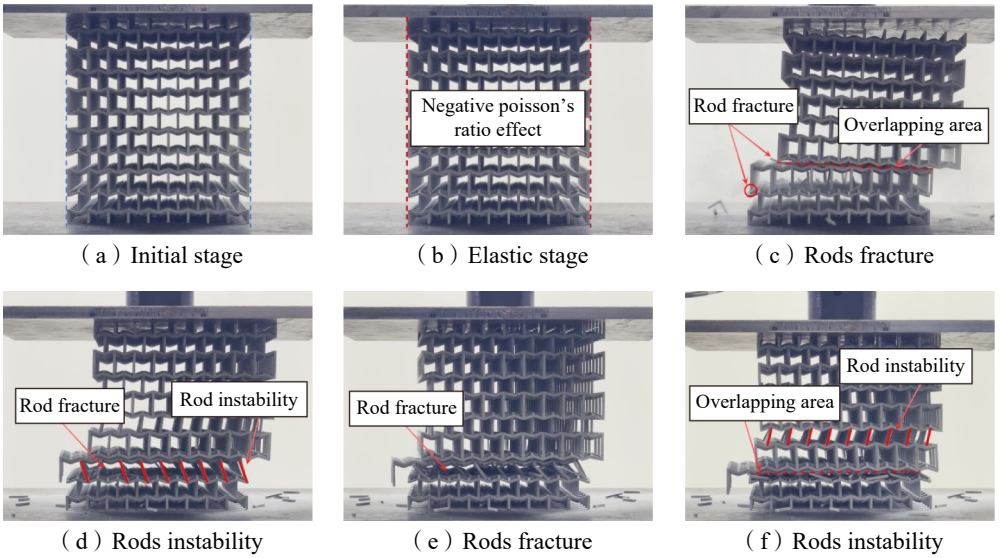


Fig.4 Stress-strain curve for plate-frame honeycomb

1.3.2 Truss honeycomb

Fig.5 shows the compressive deformation process of the truss honeycomb. At the initial phase of compression, it undergoes elastic deformation. Due to the concave angle, when compressed, the tilted rods rotate around their intersections with vertical rods, causing cell shrinkage and a negative Poisson's ratio effect. As the stress rises, the vertical rods in the middle layer of the honeycomb reach a critical pressure, fracture, and the whole cell layer collapses in one direction. Instantaneously, the honeycomb collapses and detaches from the upper plate. With continuous compression, another layer of vertical rods becomes unstable



（a）Initial stage　（b）Elastic stage　（c）Rods fracture

（d）Rods instability　（e）Rods fracture　（f）Rods instability

Fig.5 Deformation process of truss honeycomb

and fractures, leading to a similar collapse. Generally, the truss honeycomb's vertical struts tend to yield first, and compression collapse occurs layer by layer.

The stress-strain curve of the truss honeycomb is shown in Fig.6. Unlike the plate-frame honeycomb, it lacks an obvious plateau phase. After the elastic stage, a sharp stress drop occurs due to catastrophic rod failure. Then, a new cell layer bears the stress, and the honeycomb re-enters an elastic stage until the vertical rod becomes unstable. The curve shows periodic fluctuations and sudden drops, with most deformation occurring in the elastic stage. Notably, the second stress peak during compression is lower than the first one. There are two reasons: First, as Fig.5(c) shows, when the truss honeycomb first collapses, some rods in the second layer are fractured, reducing its compressive capacity for the second compression. Second, the initial collapse splits the honeycomb, and the upper part shifts right, shrinking the contact area. The computed stress drops as the actual compressive capacity weakens. Under these combined effects, the stress-strain curve exhibits unequal peak stresses.

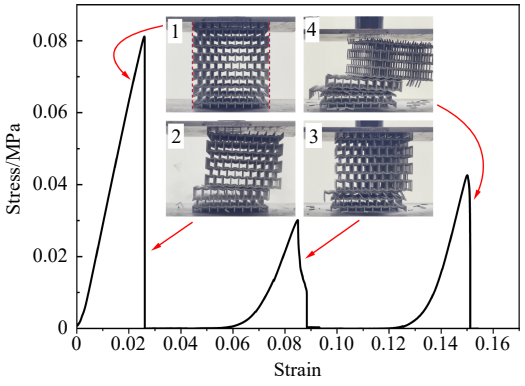
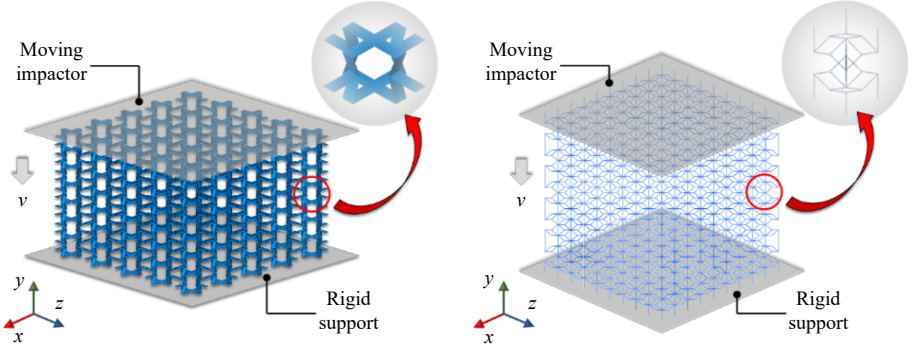


Fig.6 Stress-strain curve for truss honeycomb

2 Numerical analysis

2.1 Finite element model

To further explore honeycomb deformation characteristics and the impact of parameter changes on its performance, a finite element model was built using ABAQUS/Explicit 2022 (Fig.7). The honeycomb was sandwiched between two rigid panels, with the lower panel fixed and the upper one moving downward at a constant velocity. Self-contact of the honeycomb was set to universal, and face-to-face contact with a friction coefficient of 0.2 was defined between panels and the honeycomb. To reduce boundary effect during compression and ensure calculation convergence, the plate-frame honeycomb had 5, 7, and 5 cells in *X*, *Y*, and *Z* directions, respectively, and was modeled with S4R shell elements. The truss honeycomb had 9, 5, and 9 cells in the *X*, *Y*, and *Z* directions, respectively, and was modeled with B31 beam elements. The matrix material was nylon 12 (same as in the test), with a density of 1010 kg/m^3, Young's modulus of 1200 MPa, and yield stress of 16 MPa. An ideal elastic-plastic material model was applied to simulate the material's stress-strain relationship, assuming that the stress remains constant after the material enters the plastic phase.[31−32]



（a）Plate-frame honeycomb （b）Truss honeycomb

Fig.7 *Y*-direction compression finite element model

2.2 Validation of simulation method

To verify the finite element model's accuracy, the stress-strain curves and deformation diagrams from experiments, simulations, and theoretical analysis of the plate-frame honeycomb were compared, as shown in Fig.8 and Fig.9. In Fig.8, the experimental and simulated curves are highly consistent in the elastic region, and the overall trend is the same. In Fig.9, the compression deformation patterns of the test and the finite element model are similar: at the start of compression, the honeycomb is in the elastic stage, showing shrinkage due to the negative Poisson's ratio effect, which is concentrated in the middle. As the stress rises, the inclined walls yield. Further compression leads to plate overlapping and crushing. Therefore, it can be concluded that the numerical model is able to accurately simulate the nylon honeycomb's compression deformation and mechanical properties.

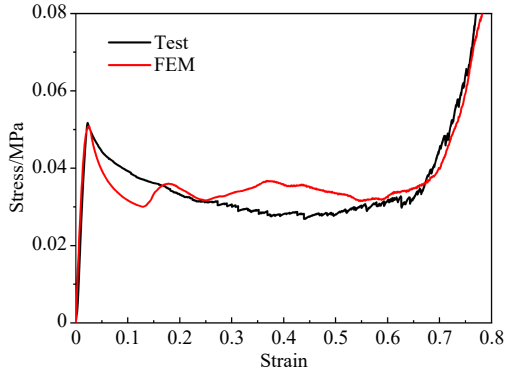


Fig.8 Stress-strain curve for plate-frame honeycomb

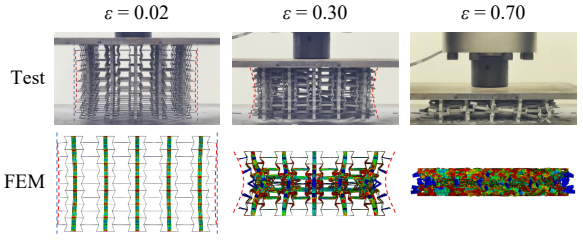


Fig.9 Comparison of deformation for plate-frame honeycomb

To boost computational efficiency without sacrificing numerical simulation accuracy, a mesh convergence analysis was performed on the finite element model. Mesh sizes of 1.0 mm, 1.5 mm, and 2.0 mm were generated and then the calculations were performed. As shown in Fig.10, the results with the mesh size of 2.0 mm fluctuated and the curve was rough, while the curves for 1.5 mm and 1.0 mm mesh sizes were relatively smooth and the results are comparable. Thus, the mesh size of 1.5 mm was selected to balance computational efficiency and accuracy.

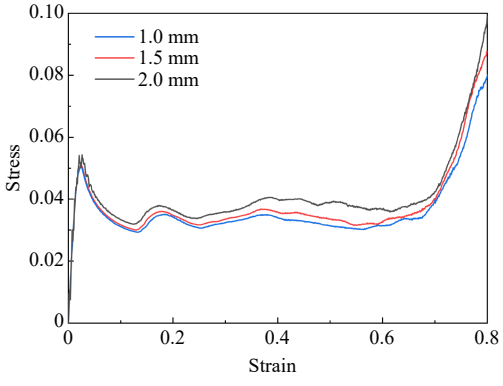


Fig.10 Mesh convergence analysis

2.3 Analysis of simulation results

2.3.1 Plate-frame honeycomb

The stress-strain curve of the plate-frame honeycomb is shown in Fig.11. Similar to experimental results, it can clearly be divided into three stages — elastic, plateau, and densification — demarcated by blue dotted lines. The red curve in Fig.11 is the energy absorption efficiency curve, where the efficiency is the ratio of the honeycomb's absorbed energy to the stress, defined as follows

$$\eta(\varepsilon)=\frac{\int_0^{\varepsilon}\sigma(\varepsilon)\,\mathrm{d}\varepsilon}{\sigma(\varepsilon)} \tag{1}$$

where η is the energy absorption efficiency, σ is the stress, and ε is the strain. The densification strain of the honeycomb is defined as the strain when the energy absorption efficiency curve starts to decline rapidly. Notably, due to the ideal boundary conditions in simulation, cell deformation occurs and the negative Poisson's ratio effect is pronounced. Besides the regular deformation of inner cells, boundary cells show insufficient deformation, which is the main reason for the stress drop from elastic peak stress to plateau stress.

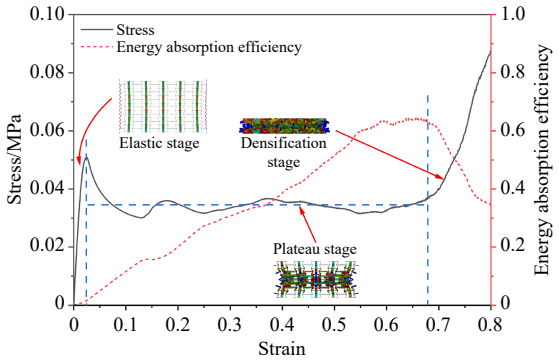


Fig.11 Numerical simulation results of plate-frame honeycomb

2.3.2 Truss honeycomb

The results of the truss honeycomb's finite element analysis are shown in Fig.12. With the elastic-plastic material constitutive model, the analysis does not simulate structural damage and extends to large strains, making up for the lack of test data on the truss honeycomb under large strains. Similar to experimental observations, the main deformation mode of the truss honeycomb is the yielding of vertical struts. During compression, it shows prominent periodic characteristics, manifested as multiple catastrophic failures with sharp stress drops. Before each collapse, the stress-strain behavior is largely linear, indicating that most of its deformation occurs within the elastic range.

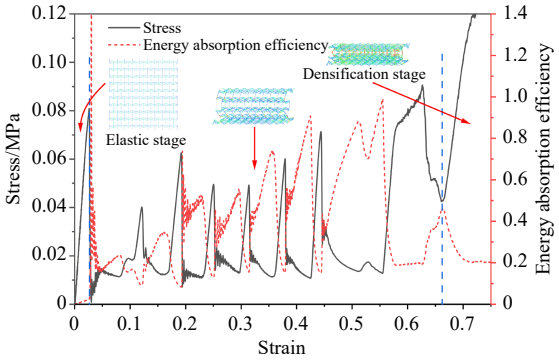


Fig.12 Numerical simulation results of trussed honeycomb

3 Results and discussion

3.1 Failure modes

Substantial disparities in mechanical properties emerged between the plate-frame and truss honeycombs, as seen in their deformation modes and stress-strain curves. Under pressure, the plate-frame honeycomb presents three distinctive stress stages—linear elastic, plateau, and densification—akin to common regular foams. In contrast, the truss honeycomb shows pronounced periodicity and no obvious plateau stage. Different failure modes were deduced from typical cell deformation.

3.1.1 Buckling of inclined walls (plate-frame honeycomb)

As shown in Fig.13(a) and Fig.14(a), during compression, the plate-frame honeycomb's inclined walls bear the brunt of the pressure. As they bend under load, cells close inward, triggering the negative Poisson's ratio effect. The shift from bending to yielding and fracturing of the inclined walls is a slow progression. Owing to the negative Poisson's ratio, cells in the same layer deform unevenly. This means cells do not fail catastrophically all at once. Thus, the plate-frame's deformation pattern demonstrates a plateau stage in the stress-strain curve.

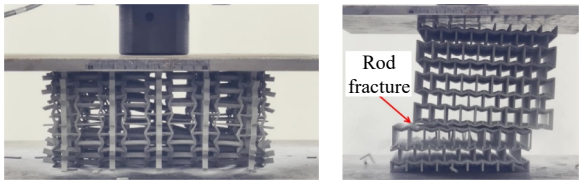
3.1.2 Instability of vertical rods (truss honeycomb)

The central vertical strut in truss honeycomb cells tends to yield first under compression. Due to the

nylon material's low plasticity before fracture, it breaks when stress hits a critical value as shown in Fig.13(b) and Fig.14(b). This strut can be modeled as a compression rod fixed at both ends, with its critical pressure F_{cr} given by the following equation

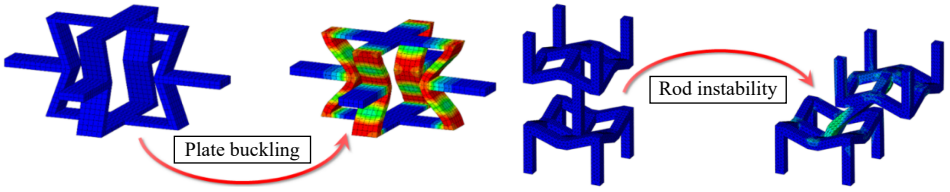
$$F_{cr} = \frac{\pi^2 EI}{(l/2)^2} \tag{2}$$

where E is the Young's modulus of material, I is the moment of inertia of the section, and l is the length of the rod. The longer the strut is, the more pronounced this phenomenon is. When the compressive stress reaches a critical value, the vertical strut yields and bends, causing displacements between cells in each layer. The additional bending moments further exacerbate the strut's deformation. Then, the whole cell layer collapses in one direction, with the stress dropping rapidly. After this layer's collapse, other layers continue to be compressed, and the cycle repeats.



（a）Plate-frame honeycomb　（b）Truss honeycomb

Fig.13 Comparison of plate frame and truss honeycomb deformation



（a）Buckling of inclined wall　（b）Instability of vertical strut

Fig.14 Deformation and damage of cell structures under compressive stress effect

3.2 Load-carrying capacity

The load-carrying capacity of a base is generally positively related to its Young's modulus. According to the general theory of porous structures, the Young's modulus of a common porous foam structure dominated by bending deformation can be written as [31]

$$\frac{E}{E_s} = C\rho_r^2 \tag{3}$$

where E_s is the Young's modulus of the substrate, ρ_r is the nominal density of the cells, and C is a variable influenced by the geometric configuration. The nominal density of the plate-frame honeycomb is

$$\rho_{r1} = \frac{V_a}{V_0} = \frac{bt\left(4l_1 + 8l_2 - b - \frac{8t}{\sin\theta}\right)}{8l_2(l_1 - l_2\cos\theta)^2 \sin\theta} \tag{4}$$

The nominal density of the truss honeycomb is

$$\rho_{r2} = \frac{V_a}{V_0} = \frac{t^2\left(l_1 + 8l_2 - \frac{t}{\tan(\theta/2)} - \frac{8t}{\sin\theta}\right)}{(l_1 - 2l_2\cos\theta)(2l_2\sin\theta)^2} \tag{5}$$

Tab.2 shows the calculated nominal density, Young's modulus, and C-value of the two honeycombs. For similar nominal densities (0.045 and 0.046), the plate-frame honeycomb has a Young's modulus nearly 270% higher than the truss honeycomb. Its $\overline{C}$-value is also larger. Moreover, the plate-frame honeycomb's stress-strain curve has a prominent plateau stress, indicating excellent load-bearing and impact resistance capabilities.

Tab.2 Plate-frame and truss honeycomb

Structure types	Nominal density	Young's modulus/MPa	C	$\overline{C}$
Plate-frame honeycomb	0.024	1.04	1.50	2.01
	0.035	3.02	2.05	
	0.045	6.03	2.48	
Truss honeycomb	0.046	1.60	0.63	0.61
	0.068	3.39	0.61	
	0.093	6.14	0.59	

Fig.15 shows the relationship between the relative Young's modulus and nominal density of honeycomb/lattice structures. Generally, 2D honeycombs have higher nominal density but weaker specific stiffness, underperforming compared to other 3D structures. According to Maxwell's stability criterion[33], the honeycombs under consideration in this paper mainly undergo bending deformation. Kelvin foam, another lattice, follows the rule that relative Young's modulus is proportional to the square of nominal density. The Ti-6Al-4V auxetic structure, similar to the truss honeycomb discussed here, has vertical pillar yielding and catastrophic failure, which can be improved by adjusting pillar aspect ratio. Ni-P Hollow-tube Micro lattices and 3D double-U auxetic structures are also bending-dominated. In contrast to the above-mentioned bending-dominated structures, the specific stiffness of the plate-frame honeycomb in this paper demonstrates a significant advantage at approximately the same relative densities. Different from the above, Octet-truss lattices are dominated by stretch deformation. At the same nominal density, the Young's modulus and initial collapse strength of the stretch-dominated lattices are typically larger than those of the bending-dominated honeycomb structures, and the stiffness of the Octet-truss lattices is superior to that of the Ni-P hollow-tube micro lattices. However, since the deformation mechanism is in the "hard" mode (stretching, compression) rather than in the "soft" mode (bending), following the initial yielding, plastic buckling or brittle collapse of the compression rod occurs, which leads to a substantial drop in stress after yielding. This renders stretch-dominated structures unsuitable for energy-absorbing applications in which a flat stress-strain curve is required.

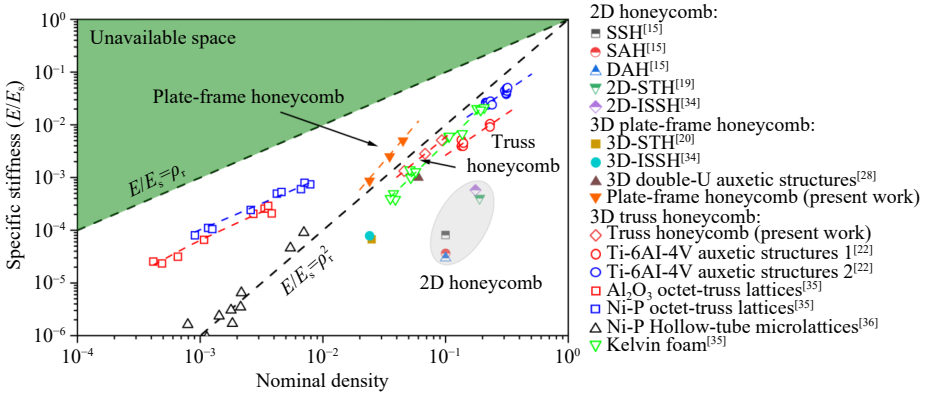
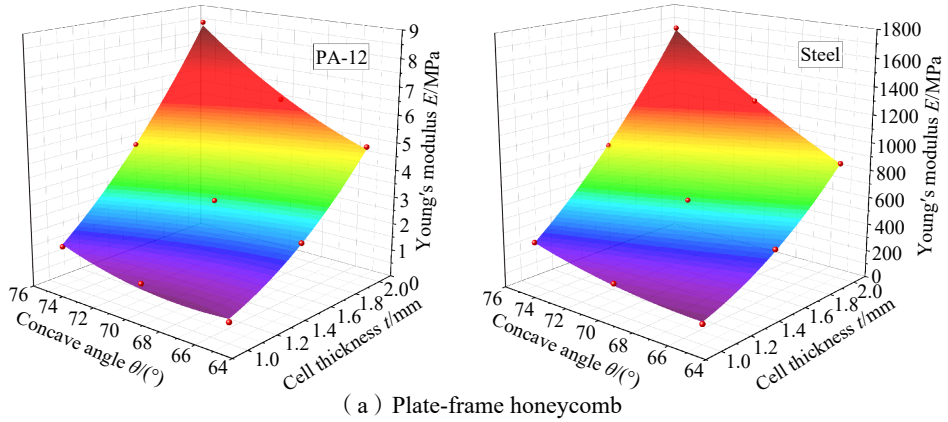


Fig.15 Specific stiffness versus nominal density for various honeycomb/lattice structures[15,19−20,22,28,34−36]

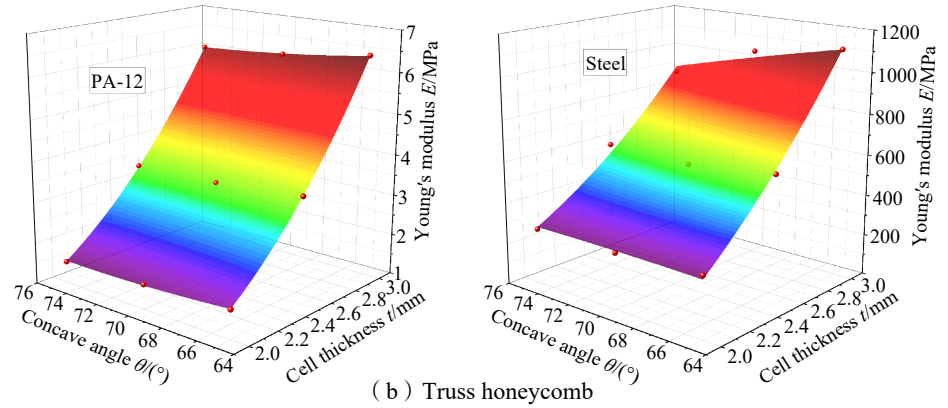
3.3 Parametric analysis

In this section, the impacts of cell angles, thicknesses, and materials on the Young's modulus and Poisson's ratio of honeycomb structures were explored through finite element simulations. The metal material is marine steel with a density of 7800 kg/m^3, a Young's modulus of 210 000 MPa, and a yield strength of 390 MPa. Fig.16 shows the Young's modulus variation of honeycomb structures with different cell angles, thicknesses and materials. For the plate-frame honeycomb, its Young's modulus rises with increasing cell

angle and plate thickness. Thicker plates mean higher nominal density, and as per Eq.(3), a structure's Young's modulus increases with nominal density. As the plate-frame cell's concave angle grows, the force arm length of the tilted wall relative to the node decreases, enabling the cell to bear more force without deforming and boosting the honeycomb's Young's modulus. Similarly, for the truss honeycomb, its Young's modulus increases when the cell angle decreases and rod thickness increases. However, it is noted that the truss honeycomb mainly depends on vertical rods to bear pressure, so the cell concave angle has a relatively small impact on its Young's modulus. The difference in materials only changes the magnitude of the Young's modulus values, and has little effect on their variation with structural parameters.



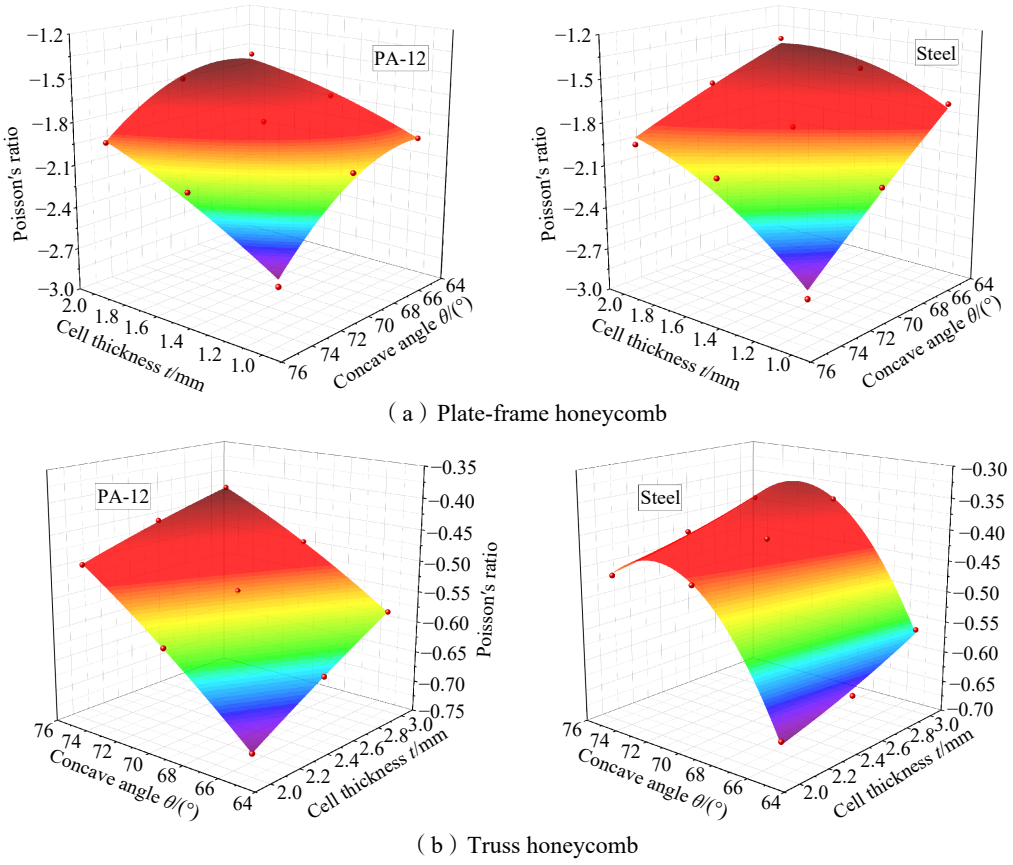
（a）Plate-frame honeycomb



（b）Truss honeycomb

Fig.16 Relationship between Young's modulus and geometric parameters

Fig.17 describes the variation law of the maximum negative Poisson's ratio of the honeycomb structure with the cell angles, thicknesses and materials. In the case of the plate-frame honeycomb, as the angle increases and thickness decreases, the negative value of the Poisson's ratio becomes more negative, and the negative Poisson's ratio effect becomes more conspicuous. For the truss honeycomb, it is evident that the angle is the primary factor influencing the Poisson's ratio of the structure. For a given angle, the variation in thickness exerts a relatively minor influence on the Poisson's ratio of the honeycomb. As the angle increases, the negative value of the Poisson's ratio decreases, and the negative Poisson's ratio effect becomes less pronounced. Overall, the range of the Poisson's ratio under different parameters for the plate-frame honeycomb is broader than that for the truss honeycomb, which implies that the plate-frame honeycomb demonstrates a superior negative Poisson's ratio effect. The variation of material does not significantly change the negative Poisson's ratio effect of the structure, which also reflects the importance of structural design.



（a）Plate-frame honeycomb

（b）Truss honeycomb

Fig.17 Relationship between Poisson's ratio and geometric parameters

4 Conclusions

This paper proposes two types of honeycombs, the 3D plate-frame and truss honeycombs, originating from the 2D re-entrant hexagon. Their deformation patterns and mechanical properties are then explored via a combination of experimental research and simulation analysis. By deeply analyzing the compression behaviors of typical cells, the differences in failure modes between the plate-frame and truss honeycombs are revealed. Furthermore, the relationship between nominal density and specific stiffness for various similar structures is comprehensively discussed. In addition, the impacts of different parameters on the Young's modulus and Poisson's ratio of the two honeycombs are analyzed. Based on these findings, some conclusions can be drawn as following:

(1) During the compression of the plate-frame honeycomb, its stress-strain curve mainly has three stages: linear elastic, plateau, and densification. It shows a significant negative Poisson's ratio effect. In contrast, the truss honeycomb lacks an obvious plateau stage. Periodic structural failures occur during compression, with its stress-strain curve featuring periodic fluctuations and sudden drops, and most of the deformation staying in the elastic range.

(2) The plate-frame and truss honeycombs have different failure modes due to the varying orientations of the re-entrant hexagon in their designs. The main failure mode of the plate-frame honeycomb is the buckling of inclined walls, while the truss honeycomb tends to first experience vertical strut instability, which is affected by the aspect ratio of the vertical strut.

(3) A comprehensive comparison of various honeycomb structures reveals that the specific stiffness of 3D honeycombs is generally better than that of 2D ones. Both 3D honeycombs under consideration are mainly subject to bending deformation, but the plate-frame honeycomb has superior specific stiffness to the truss honeycomb. For similar relative densities (0.045 and 0.046), the Young's modulus of the plate-frame honeycomb increases by nearly 270%.

(4) For the plate-frame honeycomb, its Young's modulus increases with the cell concave angle and plate thickness. For the truss honeycomb, its Young's modulus increases as the cell concave angle decreases and rod thickness rises. The truss honeycomb's Young's modulus is insensitive to concave angle changes. A larger angle in the plate-frame honeycomb leads to a more pronounced negative Poisson's ratio effect, while a larger angle in the truss honeycomb results in a weaker effect. Overall, the plate-frame honeycomb makes better use of the negative Poisson's ratio effect.

In this paper, experimental and simulation studies have been conducted on plate-frame and truss honeycomb structures. Nevertheless, several limitations still exist. For instance, the quantity of test samples is rather limited, and the fracture damage has not been taken into account when setting the simulation material properties. These limitations will be addressed in future research endeavors.

References

[1] Strek T, Matuszewska A, Jopek H. Finite element analysis of the influence of the covering auxetic layer of plate on the contact pressure[J]. Physica Status Solidi B-Basic Solid State Physics, 2017, 254(12): 1700103.

[2] Henyš P, Vomáčko V, Ackermann M, et al. Normal and shear behaviours of the auxetic metamaterials: Homogenisation and experimental approaches[J]. Meccanica, 2019, 54: 831–839.

[3] Novak N, Krstulović-opara L, Ren Z, et al. Compression and shear behaviour of graded chiral auxetic structures[J]. Mechanics of Materials, 2020, 148: 103524.

[4] Donoghue J P, Alderson K L, Evans K E. The fracture toughness of composite laminates with a negative Poisson's ratio[J]. Physica Status Solidi B-Basic Solid State Physics, 2009, 246(9): 2011–2017.

[5] Choi J B, Lakes R S. Fracture toughness of re-entrant foam materials with a negative Poisson's ratio: experiment and analysis[J]. International Journal of fracture, 1996, 80: 73–83.

[6] Imbalzano G, Tran P, Ngo T D, et al. Three-dimensional modelling of auxetic sandwich panels for localised impact resistance[J]. Journal of Sandwich Structures & Materials, 2017, 19(3): 291–316.

[7] Usta F, Türkmen H S, Scarpa F. Low-velocity impact resistance of composite sandwich panels with various types of auxetic and non-auxetic core structures[J]. Thin-Walled Structures, 2021, 163: 107738.

[8] Najafi M, Ahmadi H, Liaghat G. Experimental investigation on energy absorption of auxetic structures[J]. Materials Today: proceedings, 2021, 34: 350–355.

[9] Gao Q, Liao W H. Energy absorption of thin walled tube filled with gradient auxetic structures-theory and simulation[J]. International Journal of Mechanical Sciences, 2021, 201: 106475.

[10] Gibson L J, Ashby M F, Schajer G S, et al. The mechanics of two-dimensional cellular materials[J]. Proceedings of the Royal Society of London. Series A, Mathematical and Physical Sciences, 1982, 382(1782): 25–42.

[11] Ren X, Zhang X, Xie Y. Research progress in auxetic materials and structures[J]. Chinese Journal of Theoretical and Applied Mechanics, 2019, 51(3): 656–687.

[12] Theocaris P S, Stavroulakis G E, Panagiotopoulos P D. Negative Poisson’s ratios in composites with star-shaped inclusions: A numerical homogenization approach[J]. Archive of Applied Mechanics., 1997, 67(4): 274–286.

[13] Grima J N, Gatt R, Alderson A, et al. On the potential of connected stars as auxetic systems[J]. Molecular Simulation, 2005, 31(13): 925–935.

[14] Wang H, Lu Z, Yang Z, et al. A novel re-entrant auxetic honeycomb with enhanced in-plane impact resistance[J].

Composite Structures, 2019, 208: 758–770.

[15] Wang H, Lu Z, Yang Z, et al. In-plane dynamic crushing behaviors of a novel auxetic honeycomb with two plateau stress regions[J]. International Journal of Mechanical Sciences, 2019, 151: 746–759.

[16] Qiao J, Chen C Q. Impact resistance of uniform and functionally graded auxetic double arrowhead honeycombs[J]. International Journal of Impact Engineering, 2015, 83: 47–58.

[17] Qiao J, Chen C Q. Analyses on the in-plane impact resistance of auxetic double arrowhead honeycombs[J]. Journal of Applied Mechanics, 2015, 82(5): 051007.

[18] Wei L, Zhao X, Yu Q, et al. A novel star auxetic honeycomb with enhanced in-plane crushing strength[J]. Thin-Walled Structures, 2020, 149: 106623.

[19] Wei L, Zhao X, Yu Q, et al. Quasi-static axial compressive properties and energy absorption of star-triangular auxetic honeycomb[J]. Composite Structures, 2021, 267: 113850.

[20] Wei L, Xu S, Zhu G, et al. In-plane compression behavior of a novel 3D auxetic honeycomb[J]. Materials Today Communications, 2023, 35: 105729.

[21] Wang T, Hu J, Wang W. In-plane dynamic crushing of re-entrant triangular honeycomb with gradient thickness[J]. Materials Today Communications, 2023, 34: 105430.

[22] Yang L, Harrysson O, West H, et al. Compressive properties of Ti–6Al–4V auxetic mesh structures made by electron beam melting[J]. Acta Materialia, 2012, 60(8): 3370–3379.

[23] Beharic A, Egui R R, Yang L. Drop-weight impact characteristics of additively manufactured sandwich structures with different cellular designs[J]. Materials & Design, 2018, 145: 122–134.

[24] Guo C, Zhao D, Liu Z, et al. The 3D-printed honeycomb metamaterials tubes with tunable negative poisson's ratio for high-performance static and dynamic mechanical properties[J]. Materials, 2021, 14(6): 1353.

[25] Gao Q, Ge C, Zhuang W, et al. Crashworthiness analysis of double-arrowed auxetic structure under axial impact loading[J]. Materials & Design, 2019, 161: 22–34.

[26] Guo M, Yang H, Ma L. Design and analysis of 2D double-U auxetic honeycombs[J]. Thin-Walled Structures, 2020, 155: 106915.

[27] Yang H, Wang B, Ma L. Mechanical properties of 3D double-U auxetic structures[J]. International Journal of Solids and Structures, 2019, 180: 13–29.

[28] Yang H, Ma L. Impact resistance of additively manufactured 3D double-U auxetic structures[J]. Thin-Walled Structures, 2021, 169: 108373.

[29] Wang J, Luo X, Wang K, et al. On impact behaviors of 3D concave structures with negative Poisson's ratio[J]. Composite Structures, 2022, 298: 115999.

[30] Wang X, Wang B, Li X, et al. Mechanical properties of 3D re-entrant auxetic cellular structures[J]. International Journal of Mechanical Sciences, 2017, 131: 396–407.

[31] Zhang X, Cui H, Hu H, et al. Research on the load bearing and impact resistance of a novel structure exhibiting both positive and negative Poisson's ratios[J]. Shock and Vibration, 2024: 1–13.

[32] Ma N, Han Q, Han S, et al. Hierarchical re-entrant honeycomb metamaterial for energy absorption and vibration insulation[J]. International Journal of Mechanical Sciences, 2023, 250: 108307.

[33] Ashby M F. The properties of foams and lattices[J]. Philosophical Transactions of the Royal Society A: Mathematical, Physical and Engineering Sciences, 2006, 364(1838): 15–30.

[34] Li Q, Cao X, Wu X, et al. Investigation of the energy absorption characteristics and negative Poisson's ratio effect of an improved star-shaped honeycomb[J]. Journal of Marine Science and Engineering, 2023, 11(9): 1799.

[35] Zheng X, Lee H, Weisgraber T H, et al. Ultralight, ultrastiff mechanical metamaterials[J]. Science, 2014, 344(6190): 1373–1377.

[36] Schaedler T A, Jacobsen A J, Torrents A, et al. Ultralight metallic microlattices[J]. Science, 2011, 334(6058): 962–965.

三维板架式与桁架式蜂窝力学性能试验与数值研究

李乾宁[1,2,3], 徐林志[3], 张以恒[1,2,3], 胡鹏程[1,2,3], 武文华[4], 李春宝[1,2,3], 陈　威[1,2,3], 李　谱[5,6], 李晓彬[1,2,3]

（1. 武汉理工大学 船舶冲击损伤与安全防护重点学科与技术研究中心, 武汉 430063; 2. 武汉理工大学 船舶冲击与防护湖北省重点学科实验室, 武汉 430063; 3. 武汉理工大学 船海与能源动力工程学院, 武汉 430063; 4. 大连理工大学工业装备结构分析优化与 CAE 软件全国重点实验室, 辽宁 大连 116024; 5. 中国舰船研究设计中心, 武汉 430064; 6. 船舶振动与噪声国家重点实验室, 武汉 430033）

摘要: 随着蜂窝结构在船舶防护领域的广泛研究, 各类三维蜂窝结构不断涌现。为探究不同构型三维蜂窝的特性, 并为未来的结构设计提供思路, 本文对三维板架式和桁架式蜂窝的力学性能进行了试验与数值分析。试验样本由尼龙制成, 通过激光烧结工艺增材制造。对样本进行准静态压缩试验, 以研究三维板架式和桁架式蜂窝在变形行为模式上的差异。并通过深入分析两种蜂窝在压缩过程中典型单元的变形行为, 揭示了其失效模式的不同。鉴于结构的承载能力与其密度之间存在关联, 本文在对这两种蜂窝进行研究的同时, 还探索了各种典型的二维和三维结构的相对刚度与相对密度之间的关系。文章最后对结构进行了参数分析, 以探究内凹角度和单元厚度对力学性能的影响。

关键词: 多孔结构; 压缩试验; 增材制造; 负泊松比; 板架式与桁架式蜂窝

中图分类号: U663.7　　**文献标识码:** A

基金项目: 工业装备结构分析优化与 CAE 软件全国重点实验室（GZ25121）; 船舶振动与噪声国家重点实验室（6142204220301）

作者简介: 李乾宁（2001−）, 男, 硕士;

李春宝（1988−）, 男, 讲师, 通讯作者, E-mail: leecubao@whut.edu.cn。